Land Surface Temperature Trends Over Central and Southern Europe: Derivation and Analyses of Long-Term (1986–2018) Monthly Maxima

Christina Eisfelder, Philipp Reiners, and Claudia Kuenzer

***Abstract*—Monitoring long-term land surface temperature (LST) time series and analyzing their anomalies and trends are essential for understanding spatial patterns of global warming, particularly in Europe—the fastest-warming continent. In this study, we derived and analyzed monthly maximum LST trends over central and southern Europe at 1 km^2 resolution from advanced very high resolution radiometer-based TIMELINE LST data for the period 1986–2018. We found that almost 40% of the study area exhibited statistically significant ($p<0.1$) positive LST trends. Strongest trends were observed in eastern Europe. Additional hotspots were found on the British Isles, in southern Germany and northern Italy. Comparison of the observed LST trends with ERA5 skin temperature (SKT) trends showed that the climatological patterns correspond well. Both datasets reveal statistically significant warming trends, though with different magnitudes (LST: +0.80 ± 0.16 K/decade, SKT: +0.50 ± 0.08 K/decade). We further analyzed the LST trends with respect to different land cover classes and elevation ranges. The highest positive LST trends are observed for urban areas, grasslands, and bare areas. Croplands, which constitute more than half of the land area, also showed average trends of >0.5 K/decade and thus significantly contribute to the overall surface warming. In contrast, forested areas showed lower LST trend magnitudes (<0.5 K/decade) and a smaller share of areas with significant trends. With respect to elevation, our results revealed the lowest LST trends below 50 m and at mid-elevation ranges (750–1250 m). Both the magnitude of LST trends and the percentage area with significant trends rise towards both lower and higher altitudes. These results help to understand current warming patterns and demonstrate that long-term, high-resolution LST datasets can be used to study land-climate interactions in depth.**

***Index Terms*—Advanced very high resolution radiometer (AVHRR), climate change, elevation, Europe, land cover, land surface temperature (LST), remote sensing, trend analysis.**

Received 7 August 2025; revised 29 November 2025; accepted 10 February 2026. Date of publication 18 February 2026; date of current version 6 March 2026. This work was supported by the German Aerospace Center (DLR) TIMELINE Project. *(Christina Eisfelder and Philipp Reiners are co-first authors.) (Corresponding author: Christina Eisfelder.)*

Christina Eisfelder is with German Remote Sensing Data Center (DFD), German Aerospace Center (DLR), 82234 Wessling, Germany (e-mail: christina.eisfelder@dlr.de).

Philipp Reiners is with the Helmholtz Center Potsdam, GFZ German Research Center for Geosciences, 14473 Potsdam, Germany (e-mail: philipp.reiners@gfz.de).

Claudia Kuenzer is with German Remote Sensing Data Center (DFD), German Aerospace Center (DLR), 82234 Wessling, Germany, and also with the Department of Remote Sensing, Institute of Geography and Geology, University of Würzburg, 97074 Würzburg, Germany (e-mail: claudia.kuenzer@dlr.de).

Digital Object Identifier 10.1109/JSTARS.2026.3666131

I. Introduction

LAND surface temperature (LST) is an important aspect of Earth's climate, affecting ecosystems and organisms from local to global scales. It is recognized as one of the essential climate variables (ECV) [1], is a crucial parameter for climate models [2], and an important indicator for climate change [3]. LST represents the radiative skin temperature (SKT) of the land surface resulting from long- and shortwave radiation fluxes on one side, and turbulent heat fluxes and the ground heat flux on the other side. LST is strongly linked to the near-surface air temperature and can be used for monitoring the global warming taking place on our planet over the last few decades [4], [5].

Spatially continuous LST information can be retrieved from satellite remote sensing. Remote sensing facilitates repeatable observation over large areas and has become a standard in monitoring land surfaces. The majority of previous LST studies were conducted using data from the moderate resolution imaging spectroradiometer (MODIS) [2], [4]. MODIS has been available since its launch in 2000. With its expected decommission this year, its time series is limited to 24 years. However, monitoring climate-relevant LST changes and trends requires long time series of at least three decades [4], [6], [7]. Such long time series can be derived from the advanced very high resolution radiometer (AVHRR). The AVHRR sensor series (AVHRR-1, 2, and 3) has been operated on board 14 National Oceanic and Atmospheric Administration (NOAA) satellites and three meteorological operational (MetOp) satellites and is the only satellite sensor that has been providing spatially and temporally continuous measurements on a daily temporal resolution for over 40 years.

Within the TIMELINE project ("Time Series Processing of Medium Resolution Earth Observation Data Assessing Long-Term Dynamics in our Natural Environment") of the German Remote Sensing Data Center (DFD) at the German Aerospace Center (DLR), a homogeneous multidecadal time series from AVHRR data, starting in the early 1980s, has been generated [7]. A comprehensive range of higher-level (Level 3) land and atmosphere products is developed, including normalized difference vegetation index (NDVI) [8], Snow Cover [9], Fire Hotspots [10], Burnt Area [11], LST [12], Sea Surface Temperature [13], and Cloud Properties [14]. The TIMELINE products offer the unique possibility to investigate LST time series over Europe and North Africa based on a consistent time series covering almost

four decades at a spatial resolution of 1 km [12]. The TIMELINE LST product is the only European-wide product providing LST time series at this high spatial resolution for such a long time period. The LST time series has been corrected for orbit drift and therefore represents the daily maximum LST [15]. Based on this, the Level 3 LST product provides daily, 10-day, and monthly composites of LST.

As thermal infrared (TIR) remote sensing is limited by its inability to retrieve LST under clouds, TIR-based time series often contain significant data gaps [16]. Although statistical gap-filling methods can partially address this issue, they cannot fully reconstruct realistic climatological conditions under cloud cover [17]. This is primarily because of the absence of solar radiation, which leads to fundamentally different LST values from those under clear-sky conditions [18]. Therefore, in this study, we based our trend analyses on monthly maximum LST, which provides a more robust and climatologically meaningful measure [19]. Maximum LST values are typically observed during clear-sky conditions, and thus are a quantity that can be observed solely with TIR remote sensing.

Besides this practical advantage, temperature extremes themselves are important indicators of climate change. Climate indices such as TX90p (the percentage of days when the daily maximum temperature exceeds the 90th percentile) and the Warm Spell Duration Index (the number of days in periods of at least six consecutive days where the daily maximum exceeds the 90th percentile) are commonly used to monitor extreme heat events [3], [20]. Moreover, heatwaves can be conceptualized as a more or less persistent anomaly of maximum LST over time. Thus, positive trends in monthly maximum LST can be an indicator for both the increasing intensity and frequency of heatwaves.

Analyses of monthly maximum LST trends are especially relevant across Europe, as the European continent is a hotspot of global warming. Europe has experienced a temperature increase of approximately 2.3 K above preindustrial levels, while the global average increase was 1.5 K [21]. This makes Europe one of the fastest warming continents [22]. Land cover changes such as deforestation, urbanization, and agricultural intensification have contributed to local warming trends by changing the surface energy balance [21]. In parallel, rising temperatures have placed increasing stress on ecosystems, for instance, on forests, which are now more vulnerable to bark beetle pests [23]. Overall, the ongoing climate change has the potential to shift the distribution and composition of flora and fauna across European ecosystems. In addition, the frequency and intensity of heatwaves have risen notably in recent years [24], [25]. In 2023, Europe experienced its second warmest year on record until then, with an annual average temperature 1.02 K above the 1991–2020 average, and 2.6 K above the preindustrial level (1850–1900) [21]. Especially in urban areas those heatwaves are posing severe health threats to vulnerable groups such as the elderly and young children. According to the Copernicus 2024 climate report, Europe experienced its warmest year in 2024 with record-breaking surface warming in southern and eastern regions [22]. The identification and monitoring of LST trends are required to understand ongoing global warming and provide information for preventive or adaptive urban or land management measures. Despite the high importance of monitoring temperate increase across Europe, a recent literature review reported only three LST trend studies covering study areas within Europe [4]. Another previous review also found few studies in European countries, while most studies were conducted in the USA and China, often focusing on urbanization [2]. Recent studies on LST trends in Europe have examined their relationship with land cover and elevation [26], [27]. These analyses are important for understanding impacts of temperature change, but covered only small study areas. The primary data source in previous LST studies globally were MODIS data, followed by Landsat data. AVHRR data have rarely been applied for LST trend analyses [2], [4].

Current research gaps exist with respect to analyzing spatially detailed large-area LST trends across Europe. This is important to better understand impacts across diverse regions and relation to different land cover. Furthermore, AVHRR data, which are highly suitable for trend analyses due to their long data availability, have been underrepresented in previous studies and deserve increased investigation.

With this study, we contribute to a better understanding of LST trends across Europe. The availability of the AVHRR-based TIMELINE LST time series at only 1 km spatial resolution allows for spatially detailed analyses of long-term LST trends. Our study addresses the following main research questions.

1) What trends do we observe based on TIMELINE monthly maximum LST and how do they compare to ERA5 SKT trends?
2) Are there differences in LST trends for different land cover classes?
3) How do LST trends in central and southern Europe vary depending on elevation?

The rest of this article is organized as follows. Section II describes the data employed and the study area in central and southern Europe. Section III presents the methodology. We derived and validated gap-free monthly maximum LST time series based on the TIMELINE LST data. We then calculated LST anomalies and trends for the study area and compared the TIMELINE LST trends with trends derived from ECWMF ERA5 SKT. To contribute to a better understanding of the ongoing global warming in Europe, we further analyzed the LST trends for areas with specific land cover classes and for different elevation ranges. Section IV presents the results of the gap-filling validation and of the monthly maximum LST trend analyses. A discussion of the error budget of the monthly maximum LST time series and comparison with ERA5 and previous studies are included in Section V. This section also addresses implications of the LST trend results as well as limitations of the research and an outlook. Section V concludes this article.

II. Data and Study Area

A. TIMELINE LST

Monthly maximum LST trends were derived from the TIMELINE Level 3 LST product, which provides daily, 10-daily, and monthly LST composites from AVHRR sensors at a 1-km

spatial resolution [28]. The TIMELINE monthly LST product includes a variable representing the monthly maximum LST, computed as the maximum of all valid daily maximum LST observations within each month [28]. The generation of the monthly maximum values involved additional quality filtering: all daily LST observations that deviated by more than four times the standard deviation of the respective month were excluded to remove outliers. Furthermore, observations with a satellite zenith angle exceeding 50° and LST values greater than 340 K—considered physically unrealistic—were filtered out during Level 3 product generation [12], [15]. The TIMELINE Level 3 LST product also contains an uncertainty layer quantifying the retrieval uncertainty of the monthly maximum LSTs. For this study, LST pixels with an uncertainty $\geq$ 2.5 K were removed.

B. ERA5 Land SKT

The ERA5-Land reanalysis dataset, provided by the European Centre for Medium-Range Weather Forecasts, is among the most widely used and established data sources for studying global and regional climate change. It provides a range of land surface variables from 1950 to the present at an hourly temporal resolution and a spatial resolution of approximately 9 km. The reliability of ERA5 temperature data over Europe has been demonstrated in several studies, showing strong performance [49], [50]. The SKT variable represents the temperature of the uppermost surface layer and is considered physically equivalent to LST. In this study, the climatology of the TIMELINE LST as well as the spatial distribution of the trends were compared to SKT data. For this purpose, the daily SKT at 13:00 was downloaded.

C. TIMELINE NDVI

The TIMELINE NDVI product provides homogeneous NDVI time series from AVHRR sensors starting in the early 1980s over Europe and North Africa at a 1-km spatial resolution [8]. The TIMELINE Level 3 NDVI product includes daily, ten-day, and monthly NDVI composites that were generated by applying a median compositing approach [29]. In this study, NDVI data were required for the random forest (RF) regression model used for gap-filling in the monthly maximum LST datasets. A key predictor in the RF model was the long-term monthly NDVI at each corresponding pixel. This long-term NDVI was calculated for each month as the mean of the monthly NDVI composite time series for 1986–2018 from the TIMELINE NDVI product. Since all TIMELINE products share a common data structure with identical spatial resolution, extent, and projection, no adjustments to resolution or projection were necessary.

D. Elevation Data

Another predictor used in the gap-filling model is elevation. The elevation information was derived from the Global Multi-resolution Terrain Elevation Data 2010 (GMTED2010) [30]. This dataset has a native resolution of 1 km and was projected into the LAEA-ETRS89 coordinate system to match the projection of the TIMELINE LST product.

E. ESA CCI Land Cover Classifications

Land cover information is utilized in this study to analyze monthly maximum LST trends for different land cover types. For this purpose, the ESA Climate Change Initiative (CCI) land cover products, which are available annually and cover the period from 1992 to 2018, were applied. From these datasets, stable land cover pixels were derived using the approach described in [31]. The original ESA-CCI dataset distinguishes 37 land cover classes. In this study, these were aggregated into ten broader categories: Cropland, Mosaic Cropland, Broadleaf Forest, Needleleaf Forest, Mixed Forest, Shrubland, Grassland, Sparse Vegetation, Urban Area, and Bare Area. To ensure spatial compatibility with the TIMELINE LST dataset, the land cover data with an original spatial resolution of 300 m were resampled to 1 km using a maximum area fraction approach. Finally, stable land cover pixels over time were identified, by selecting only those pixels that were assigned the same land cover class in all years from 1992 to 2018. The area with stable land cover pixels covers about 91% of the study.

F. Study Area

The study area is located between 35°N and 56°N latitude and 10°W and 30°E longitude, including central, western, southern, and south-eastern Europe. This area is determined by the availability of daytime corrected LST [15], which, in turn, is determined by the extent of the Annual Cycle Parameters from SEVIRI LST [32] used for the daytime correction.

Fig. 1 shows the geographical extent and relevant characteristics of the study area. Fig. 1(a) shows the average maximum LST in May, for which a gradient from generally lower temperatures in the North to higher temperatures towards the South of the study area can be observed. May was selected for this figure because it provides good contrast within the study area and represents moderate temperatures between the annual minimum and maximum for Europe [22]. Fig. 1(b) presents the distribution of stable land cover pixels derived for this study (see Section II-E). The most prevalent land cover in Europe is cropland, spreading over more than 50% of the study area [see Fig. 1(e)]. Different types of forests, which cover almost 30% of the study area, are distributed all over the region. Grassland is mainly located in central and western Europe, with a main distribution area on the British Isles, and covers about 10% of the study region. An elevation map is provided in Fig. 1(c), as well as a diagram showing the area distribution for the elevation classes in Fig. 1(d). More than half of the study area lies below 250 m and 90% below 1000 m height above sea level. Major mountain ranges within the study area are the Alps, the Pyrenees, and the Carpathians.

III. Methodology

A. Gap Filling and Anomaly Calculation

To address gaps in the monthly LST product, a two-step gap-filling approach—comprising spatial and temporal

TABLE I
DATASETS UTILIZED IN THIS STUDY

Product name	Spatial resolution	Temporal resolution	Period used	DOI/Link
TIMELINE LST Level 3	1 km	monthly	1986–2018	DOI: 10.15489/rnnvbugzmh44
TIMELINE NDVI Level 3	1 km	monthly	1986–2018	DOI: 10.15489/y61jgjjj3x15
ERA5-Land hourly data from 1950 to present → SKT	9 km (0.1°)	hourly	1986–2018	DOI: 10.24381/cds.e2161bac
Global Multiresolution Terrain Elevation Data 2010 (GMTED2010)	1 km (30'')	once	2010	DOI: 10.5066/F7J38R2N
ESA CCI Land Cover	300 m	annual	1992–2018	ESA [54]

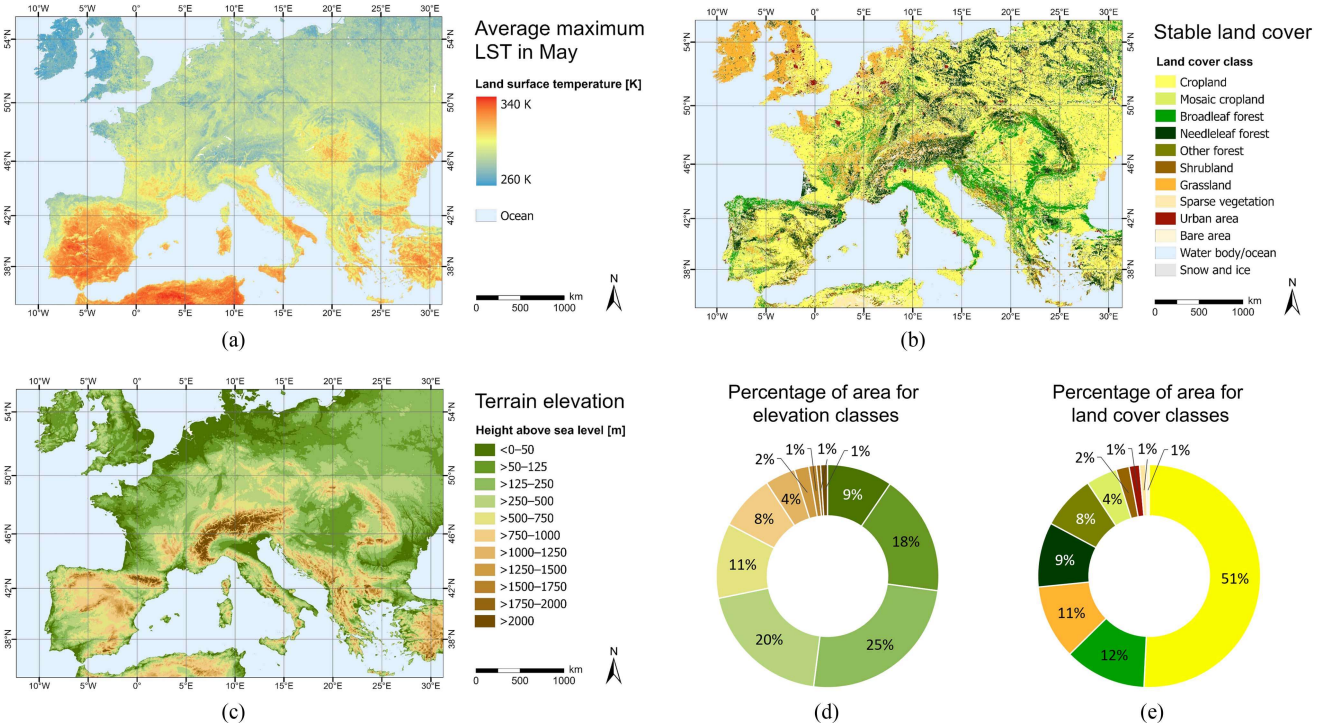

Fig. 1. Characteristics of the study area. (a) Average maximum LST in May for the period 1986–2018. (b) Stable land cover. (c) Terrain elevation. (d) Percentage of area for the elevation classes. (e) Percentage of area for the land cover classes.

interpolation—was applied to derive a continuous dataset of monthly maximum LST. Spatial gap-filling was applied directly to the monthly maximum LST values, whereas temporal gap-filling was performed on the LST anomalies. An overview on data and steps involved for gap-filling and LST anomalies time-series production is provided in Fig. 2.

1) Spatial Gap Filling: For spatial gap-filling, the study area was divided into 2° × 2° subregions. If more than 50% of the pixels within each subregion contained valid LST values, a RF regression model was set up to predict the missing values. Similar approaches for gap-filling of LST time-series with RF models were successfully applied in previous studies [33], [34]. The valid pixels were randomly split into a training and test dataset. The training data was used to fit the model, while the test data was held out for validation. The predictors of the RF Regression model were the long-term monthly NDVI derived from the TIMELINE NDVI product, the long-term monthly maximum LST and the elevation. With this approach, for most of the timesteps, spatially gap-free monthly maximum LST maps could be produced.

2) Calculation of Monthly Maximum LST Anomalies: Based on the spatially filled monthly maximum LST datasets, anomalies were computed by subtracting the long-term monthly climatology, defined as the mean value of each respective month over the study period (1986–2018). To mitigate the influence of sporadic undetected cloudy pixels and occasional sensor-related artifacts, unrealistic anomaly values—defined as absolute deviations exceeding ±15 K—were excluded. This threshold was derived through internal outlier analysis.

3) Temporal Gap Filling: Following the computation of LST anomalies, the remaining data gaps—primarily occurring

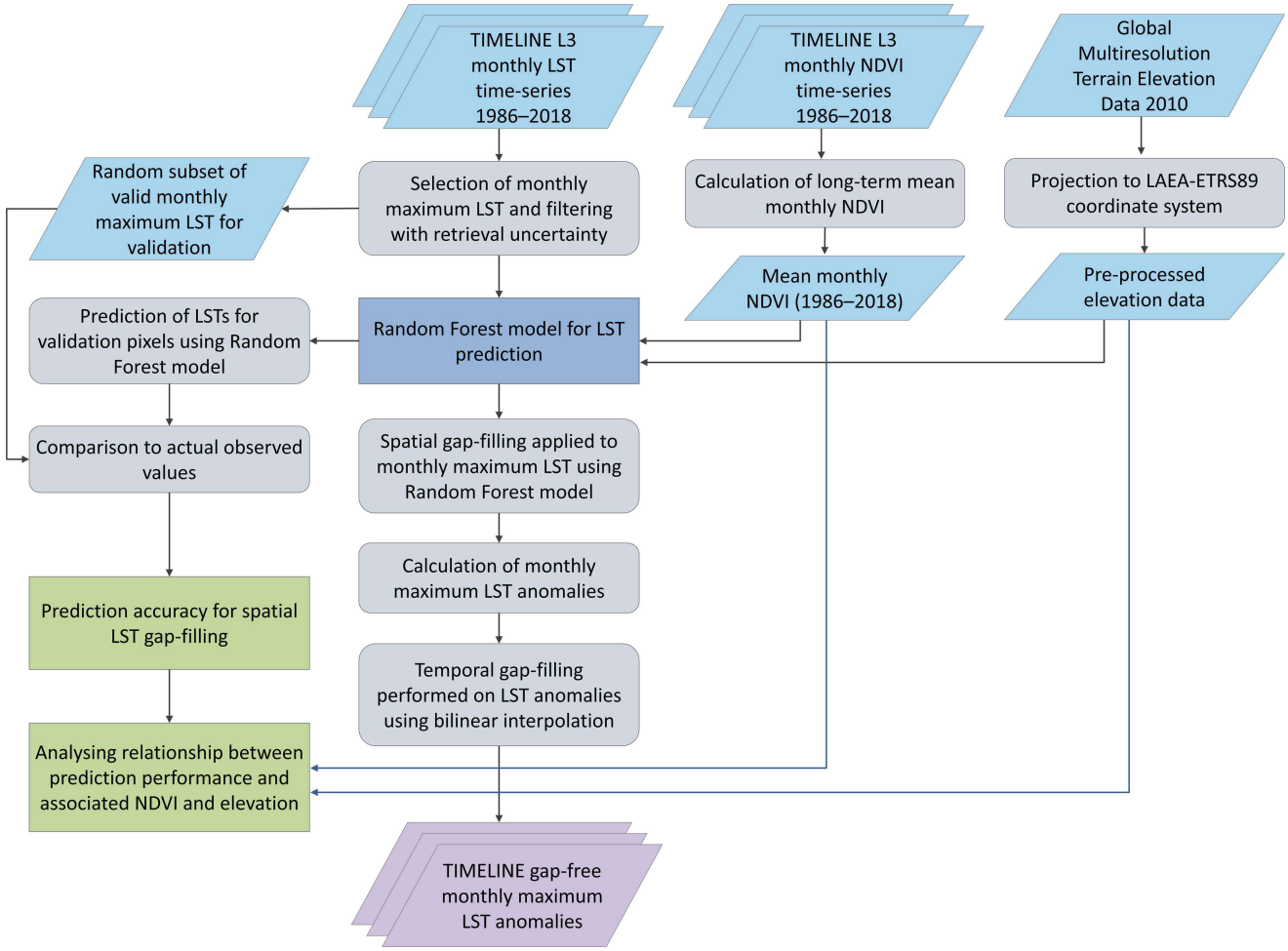

Fig. 2. Flowchart showing the data and steps for production and validation of the gap-free TIMELINE monthly maximum LST anomalies time-series. The resulting anomalies time-series is input to the monthly maximum LST trend calculation (see Fig. 3).

between November and January—were filled through interpolation. These gaps were typically associated with time steps that either contained too few valid LST observations to train an RF regression model or lacked a Level 3 LST product altogether. To address these gaps, bilinear interpolation was applied on a per-pixel basis, using the anomalies from the preceding and succeeding time steps. This ensured temporal continuity in the anomaly time series and completed the gap-filling process.

B. Calculation of Monthly Maximum LST Trends

The trend analysis was conducted for each pixel within the LST anomaly data derived from the TIMELINE monthly maximum LST time series, and consisted of three components: the Mann-Kendall trend test, the Theil-Sen slope estimation, and a subsequent confidence analysis. The Mann-Kendall trend test [35], [36] is a nonparametric method particularly suited for detecting monotonic trends. The resulting p-value indicates whether a trend is significant or not. In this study, trends were considered statistically significant for p-values lower than 0.1.

The magnitude and direction of the trend were estimated using the Theil-Sen slope estimator [37], [38]. The Theil-Sen Slope Estimator calculates the strength of a monotonic trend as the median of the slopes of the lines through all point pair combinations. It is more robust compared to simple linear regression, e.g., ordinary least squares regression, and resistant to the impact of outliers [39]. The combined application of the Mann-Kendall test and Theil-Sen estimator has proven effective in climate trend analyses and has been widely applied in recent literature [40], [41], [42], [43].

Finally, a confidence analysis was conducted to assess the statistical uncertainty of the trend estimates. This analysis returned the range of possible trend values, expressed as a confidence interval between the minimum and maximum plausible slopes for each pixel.

The resulting monthly maximum LST trends were analyzed for individual land cover classes and elevation ranges. An overview on the processing steps and analyses performed with the LST trends are provided in Fig. 3.

C. Calculation of ERA5 SKT Trends

The daily ERA5 SKT data was aggregated to monthly maximum values. Subsequently, the monthly maximum SKT datasets

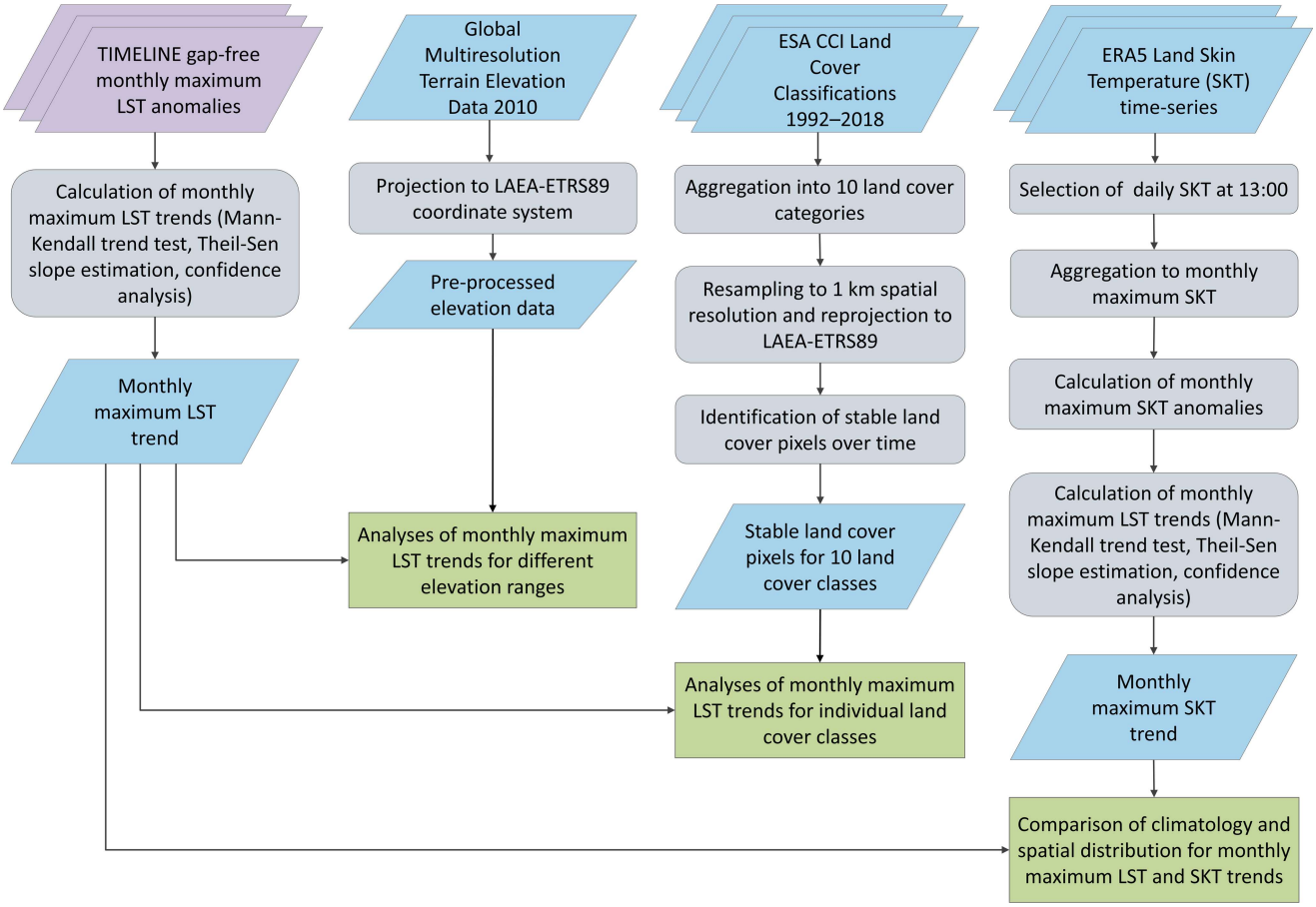

Fig. 3. Flowchart showing the data and steps for calculation of monthly maximum LST trends, analyses performed therewith regarding land cover and elevation, as well as calculation of and comparison to monthly maximum SKT trends. The input LST anomalies time-series is the outcome from the gap-filling procedure (see Fig. 2).

were spatially clipped to match the study area. Anomalies and trends were then computed following the same methodology as applied to the TIMELINE LST dataset. The steps for monthly maximum SKT trend calculation and the final comparison to the LST trends are included in Fig. 3.

D. Validation of the Spatial Gap Filling

As mentioned in Section III-A-1, during the spatial gap-filling process, a subset of valid LST values was held out for validation purposes. For these pixels, LSTs were now predicted using the RF model and subsequently compared to the actual observed values. In addition to assessing the overall prediction accuracy, the relationship between prediction performance and the associated NDVI and elevation values was also analyzed to evaluate the model's behavior regarding variation in these variables.

IV. Results

A. Results of the Gap-Filling Validation

The maps in Fig. 4 illustrate the gap-filling statistics of the LST time series for each pixel:

1) the percentage of original LST observations,
2) spatially filled LST, and
3) temporally filled LST.

The results show that, for the majority of the study area, more than 70% of the time series is composed of original LST data. A clear North-to-South gradient is visible, with a lower proportion of original observations in northern regions. This pattern can be attributed to the higher frequency of cloud cover at higher latitudes, leading to a lower number of valid LST observations.

In addition, significantly fewer original LST observations are found over mountainous regions such as the Alps and the Pyrenees. This can be attributed to the filtering of LST values with high retrieval uncertainty (see Section II-A), as the complex terrain in mountainous regions typically results in higher LST retrieval uncertainties.

Fig. 4(b) and (c) further indicates that the data gaps in the northern regions were predominantly filled using the spatial interpolation method, while the gaps in mountainous areas were mainly filled using the temporal filling method.

Fig. 5 presents percentages of original, spatially filled, and temporally filled LST values per month throughout the time series. Again, more than 75% of the LST data from March to October consist of original (observed) values. The data gaps during the winter months are predominantly filled using the

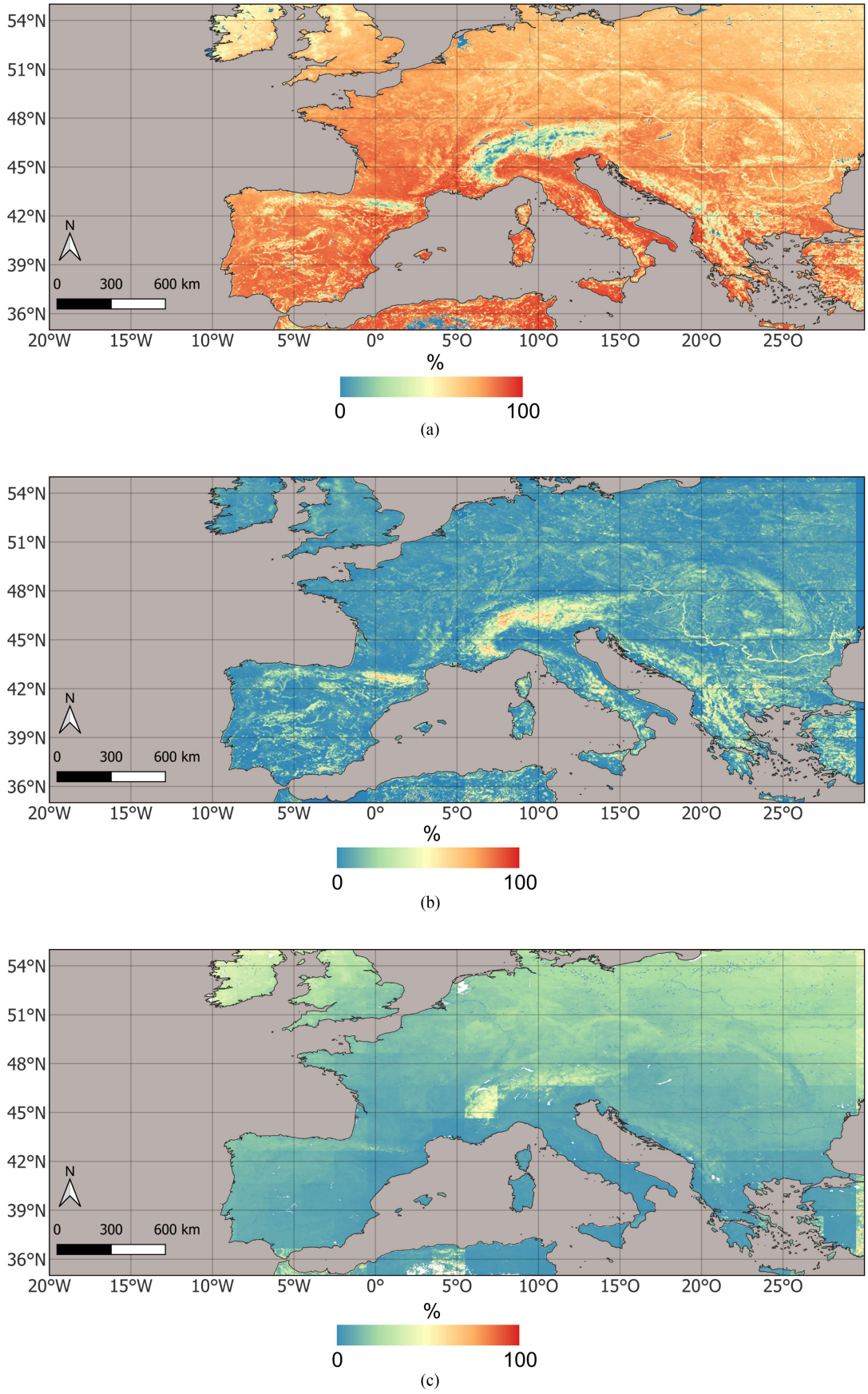

Fig. 4. Percentage of pixels in the whole time series, which were (a) original LST, (b) spatially filled, and (c) temporally filled.

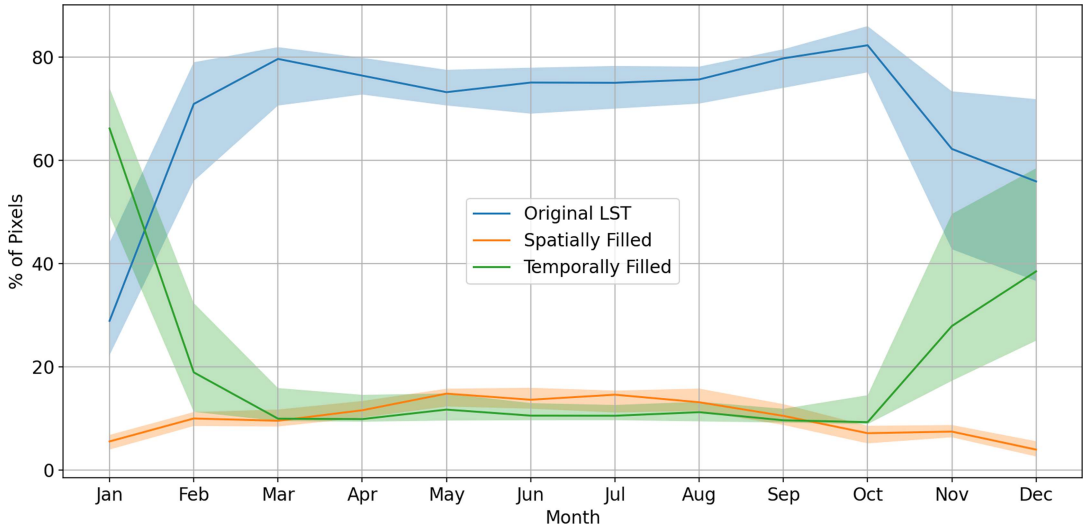

Fig. 5. Percentage of original LST, spatially filled, and temporally filled pixels per month.

temporal filling method. The proportion of spatially filled pixels increases slightly during the summer months, however it remains below 15% throughout the year.

Fig. 6 provides further details regarding the gap-filling validation. The correlation between predicted and observed LST shows an overall coefficient of determination R^2 of 0.96 [see Fig. 6(a)]. For all parameters (elevation, NDVI, month) and ranges analyzed, the average difference between predicted and observed LST is close to zero. This means that no bias arises for any of these variables. With respect to different elevation ranges, we find that the uncertainty of predicted LST increases towards higher terrain elevation [see Fig. 6(b)]. For different NDVI ranges, the LST prediction accuracy remains stable [see Fig. 6(c)]. Having a look at individual months, we find higher prediction uncertainties for summer months compared to winter months [see Fig. 6(d)].

B. Results of Monthly Maximum LST Trend Analysis

Fig. 7 presents the time series of average monthly maximum LST anomalies across the study area for the TIMELINE LST [see Fig. 7(a)] and ERA5 SKT [see Fig. 7(b)], along with the overlay of the rolling mean for both datasets [see Fig. 7(c)]. Both datasets reveal a statistically significant warming trend, however, with different magnitudes: The TIMELINE LST shows a stronger trend of $+0.80 \pm 0.16$ K/decade, while the ERA5 SKT displays a more moderate trend of $+0.50 \pm 0.08$ K/decade. Despite the differences in the trend magnitude, the climatological patterns of monthly maximum LST from TIMELINE and ERA5 correspond well. For instance, the major European heatwaves in 2005, 2007, and 2013 are clearly captured by both data sources.

Fig. 8 displays the spatial distribution of the significant TIMELINE LST trends [see Fig. 8(a)], as well as the corresponding slope [see Fig. 8(b)] and p-value [see Fig. 8(c)]. 40.4% of the land area exhibit significant trends, with 37.9% of the total area showing positive trends and 2.5% showing negative trends. The strongest positive trends can be observed in Eastern Europe, particularly on the territory of the Ukraine and Belarus and in the Hungarian Plain. Here, the trends frequently exceed 1 K/decade. Additional hotspots of positive trends can be found on the British Isles, in Southern Germany and Northern Italy, particularly in the Po Valley. In contrast, negative trends are very sparse and are primarily located in the southern part of the study area, such as on the Iberian Peninsula, in southern Italy, and Turkey.

Fig. 9 displays the results of the trend analysis conducted with the ERA5 SKT dataset. When compared to the TIMELINE LST trend analysis, several similarities as well as notable differences become visible. As with the TIMELINE LST results, the entire region exhibits predominantly positive trends [see Fig. 9(a)], mostly ranging between 0.5 and 1 K/decade, with hotspots exceeding 1 K/decade. One particularly prominent hotspot, which was also identified in the TIMELINE LST analysis, is located in Eastern Europe, spanning also parts of Ukraine, Belarus, and the Hungarian Plains.

However, several key differences can be identified. Most obviously, the ERA5 SKT results show area-wide statistically significant trends, with only a few gaps (e.g., on the Iberian Peninsula and the British Isles)—contrasting with the more fragmented pattern seen in TIMELINE LST trends. Due to the coarser spatial resolution of ERA5, the trends appear smoother, but also exhibit fewer spatial details. An additional hotspot appears along the eastern coast of Spain in the province of Valencia, which was not as prominently featured in the TIMELINE dataset. In contrast to the TIMELINE LST analysis, the ERA5 SKT data do not indicate significant trends over the British Isles.

C. Analyses of Monthly Maximum LST Trends Regarding Land Cover and Elevation

The unique combination of an LST time series spanning a climatologically relevant period of over 30 years and a relatively high spatial resolution of 1 km enables to link global warming over land with key land surface variables such as land cover and elevation. For these analyses, pixels with statistically significant

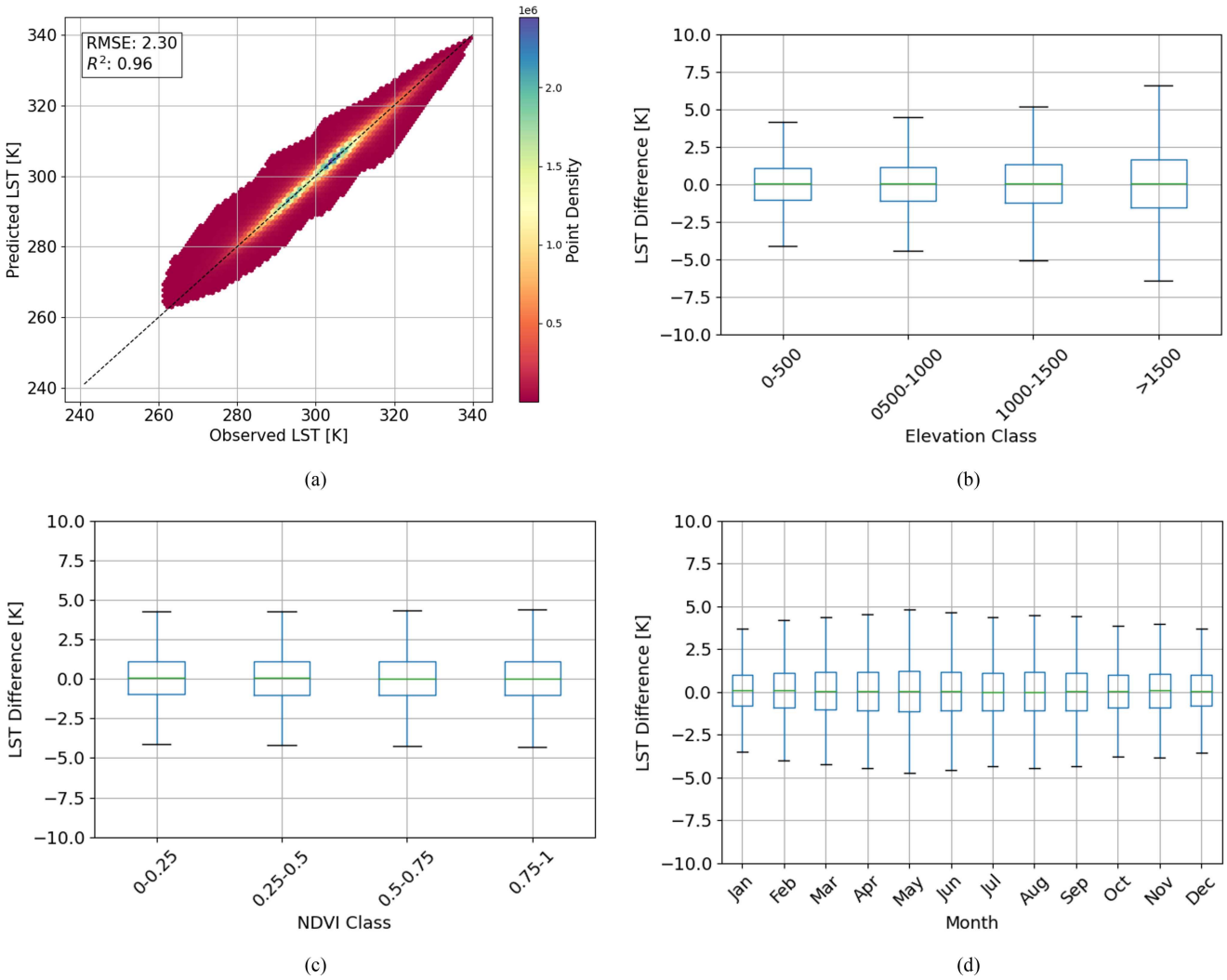

Fig. 6. Results of the gap-filling validation: (a) Predicted versus observed LST and the difference between predicted and observed LST stratified by (b) elevation range, (c) NDVI range, and (d) month.

LST trends were grouped according to the stable land cover classes derived from the ESA CCI Land Cover products (see Section II-E), and, for a separate examination, into elevation ranges.

Fig. 10 presents boxplots of the significant LST trends for each land cover class. The corresponding bars below illustrate the percentage of pixels with significant trends within each class. The results show that urban areas, grasslands and bare areas exhibit the highest positive LST trends, as well as high proportions of statistically significant trends. The high trends in the grassland class correspond with the spatial trend distribution, as grassland areas are primarily located in Eastern Europe—a region identified as a major warming hotspot.

Croplands and sparse vegetation also show average trends of >0.5 K/decade. Given the fact, that croplands constitute more than half of the land area within the study region, they contribute substantially to the overall surface warming observed in Europe. In contrast, forested areas show both lower LST trend magnitudes and a smaller share of significant trends. Shrublands and mosaic croplands also show comparatively low LST trends.

Fig. 11 shows the result of the analysis of LST trends with respect to separate elevation ranges. This analysis reveals a distinct pattern: both the magnitude of LST trends and the percentage of significant trend pixels decrease with increasing elevation between 50 m and 1000 m height. At higher elevation ranges, above 1000 m, both parameters rise again with increasing elevation. Consequently, the lowest LST trends are observed in the mid-elevation regions between 750 m and 1250 m. An exception from the general pattern are the LST trends for areas at elevations below 50 m, which are mainly located in coastal regions. Here, comparatively low LST trends can be observed.

V. Discussion

A. Error Budget of the Monthly Maximum LST Time Series

The error budget of the generated LST time series includes three main sources: retrieval errors [12], errors introduced by daytime normalization [15], and errors associated with the gap-filling methods. Therefore, it is essential that each step in the time series generation is accompanied by validation

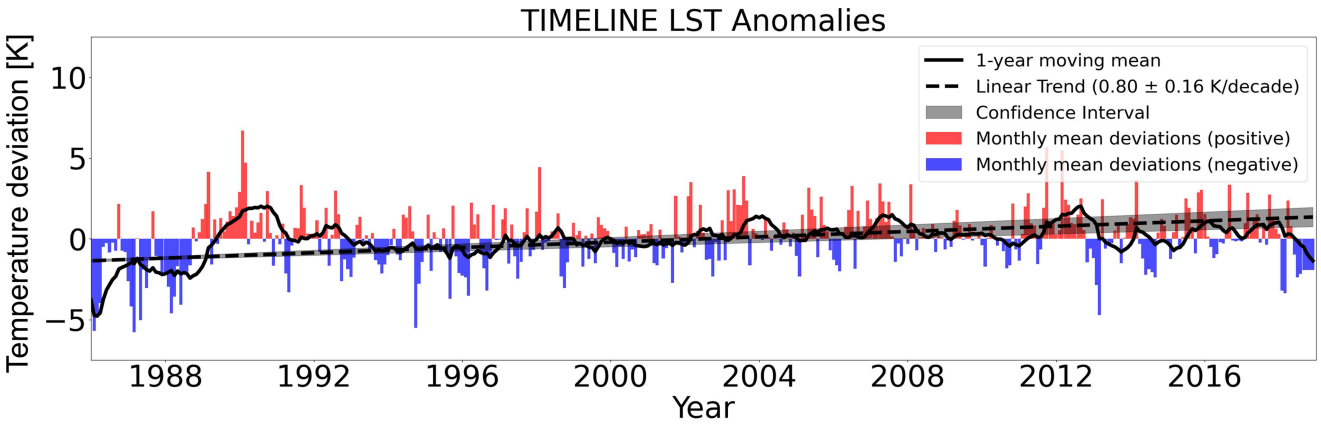

(a)

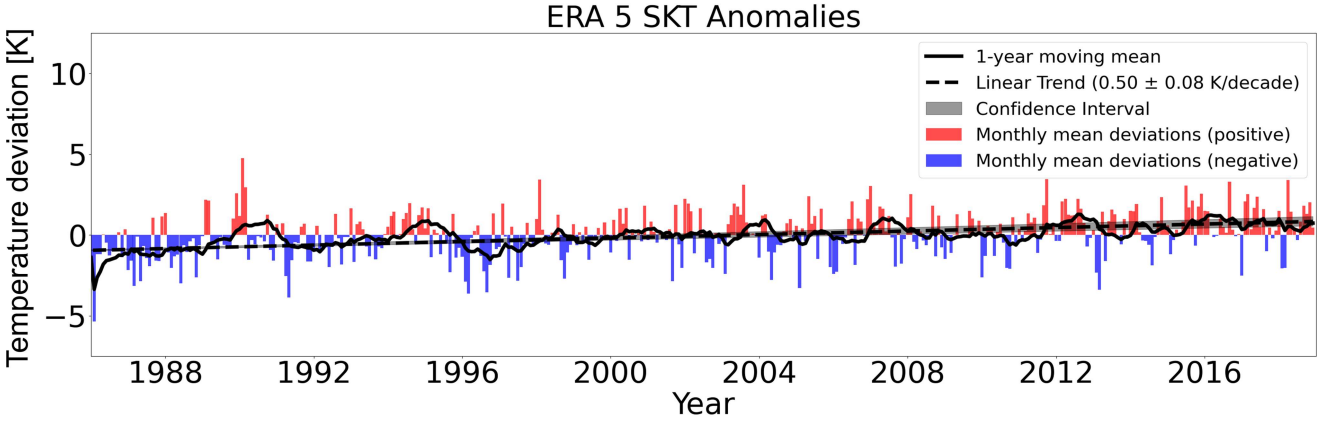

(b)

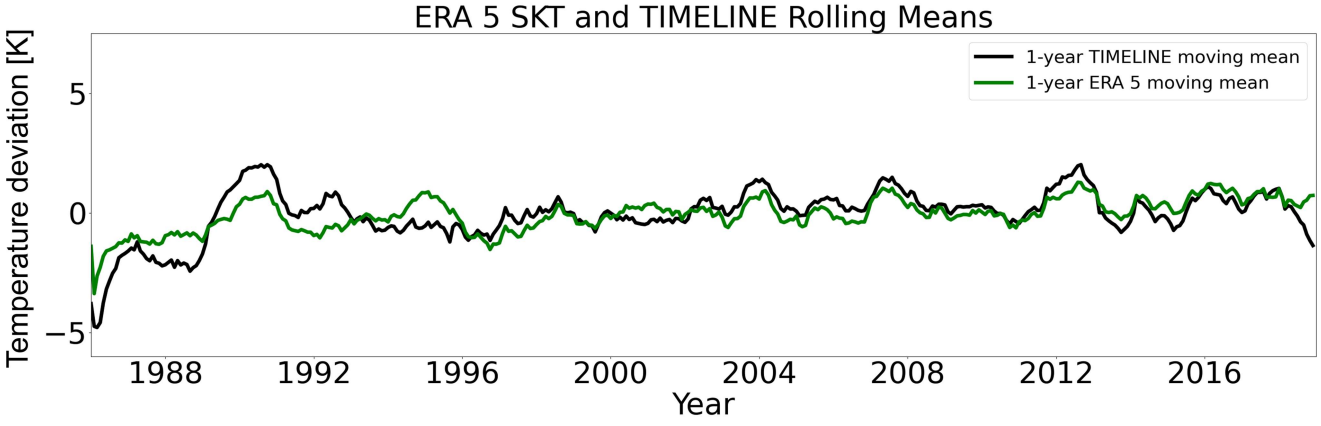

(c)

Fig. 7. Monthly maximum LST anomalies and 1-year rolling mean for (a) TIMELINE LST, (b) ERA5 SKT, and (c) overplot of the rolling means from both data sources.

procedures, which was consistently implemented in this work and the TIMELINE LST product generation. The mean retrieval uncertainty of the TIMLINE LST product is shown in Fig. 12. We observe a higher retrieval uncertainty in mountainous regions due to complex topography, snow cover variability, and a high local variability on the AVHRR (1 km) scale. Higher retrieval uncertainties in low vegetated areas, such as in Southern Europe, can be attributed to a higher uncertainty of emissivity.

The instantaneous LST was validated by comparison to both in situ LST and MODIS LST. These comparisons resulted in mean absolute differences (MADs) of 1.8 K and 2.3 K, respectively [12]. The daytime normalization was validated using CCI

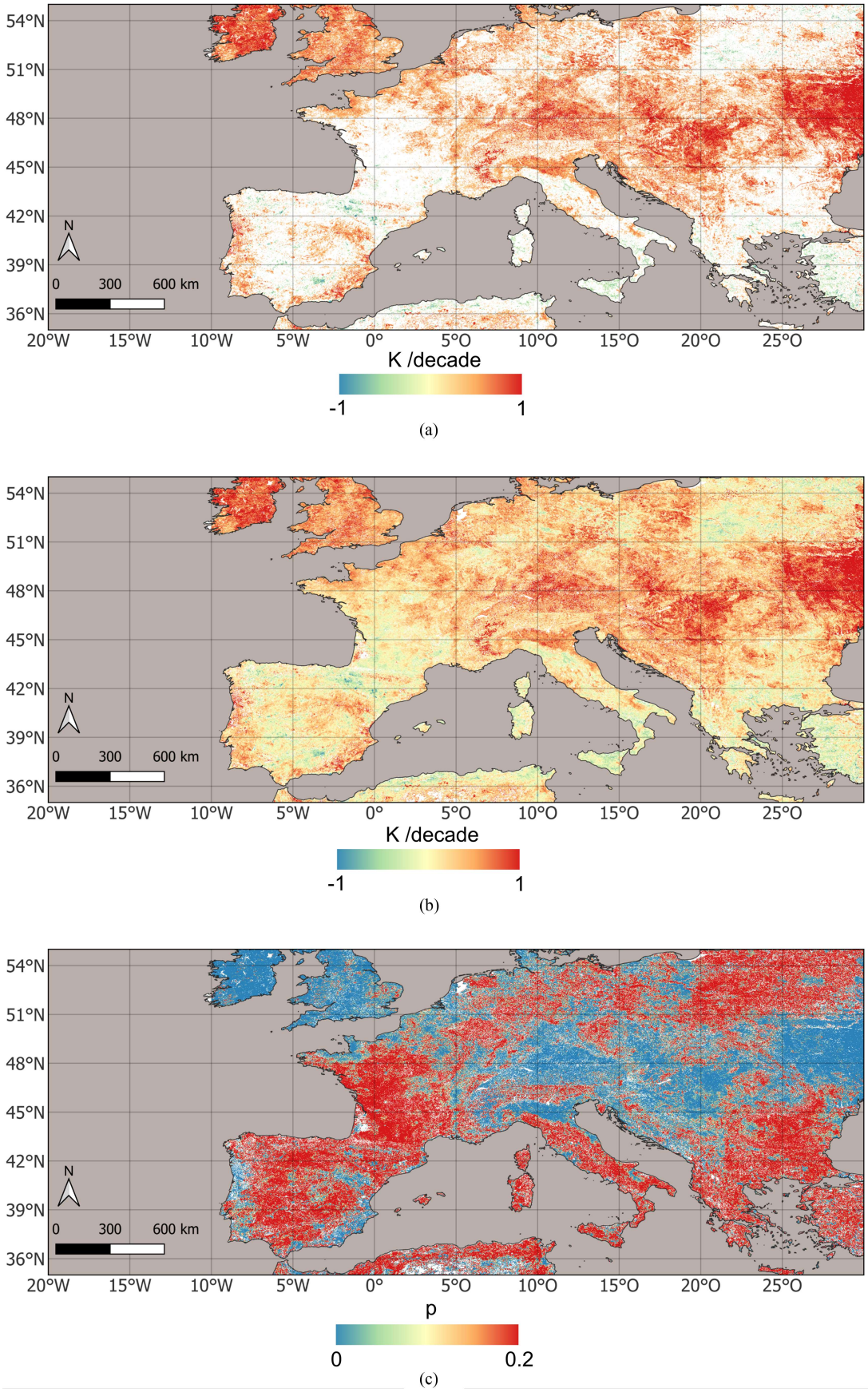

Fig. 8. Results of the monthly maximum trend analysis using TIMELINE LST. (a) Significant trends. (b) slope. (c) p-value.

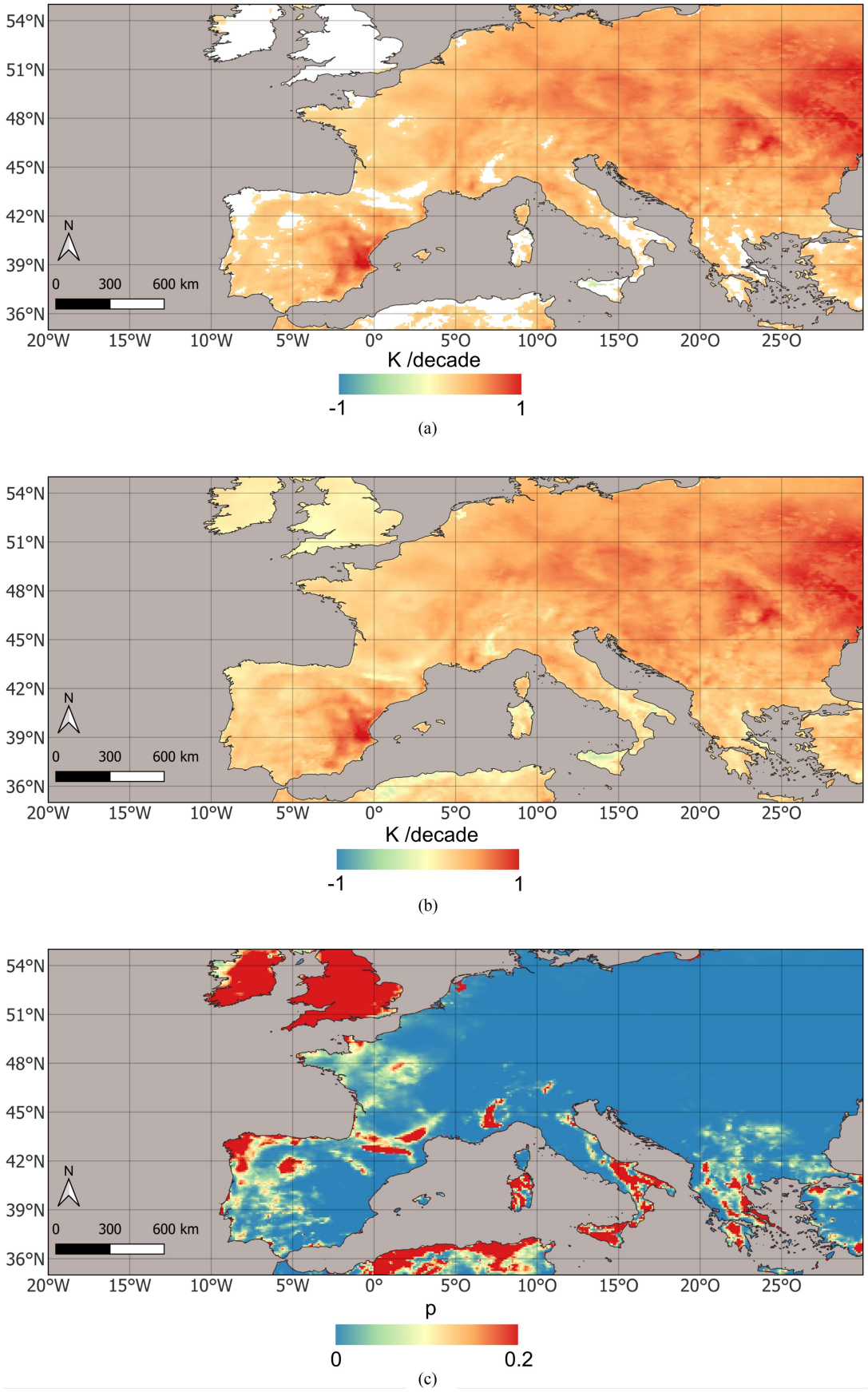

Fig. 9. Results of the monthly maximum trend analysis using ERA5 SKT. (a) Significant trends. (b) Slope. (c) *p*-value.

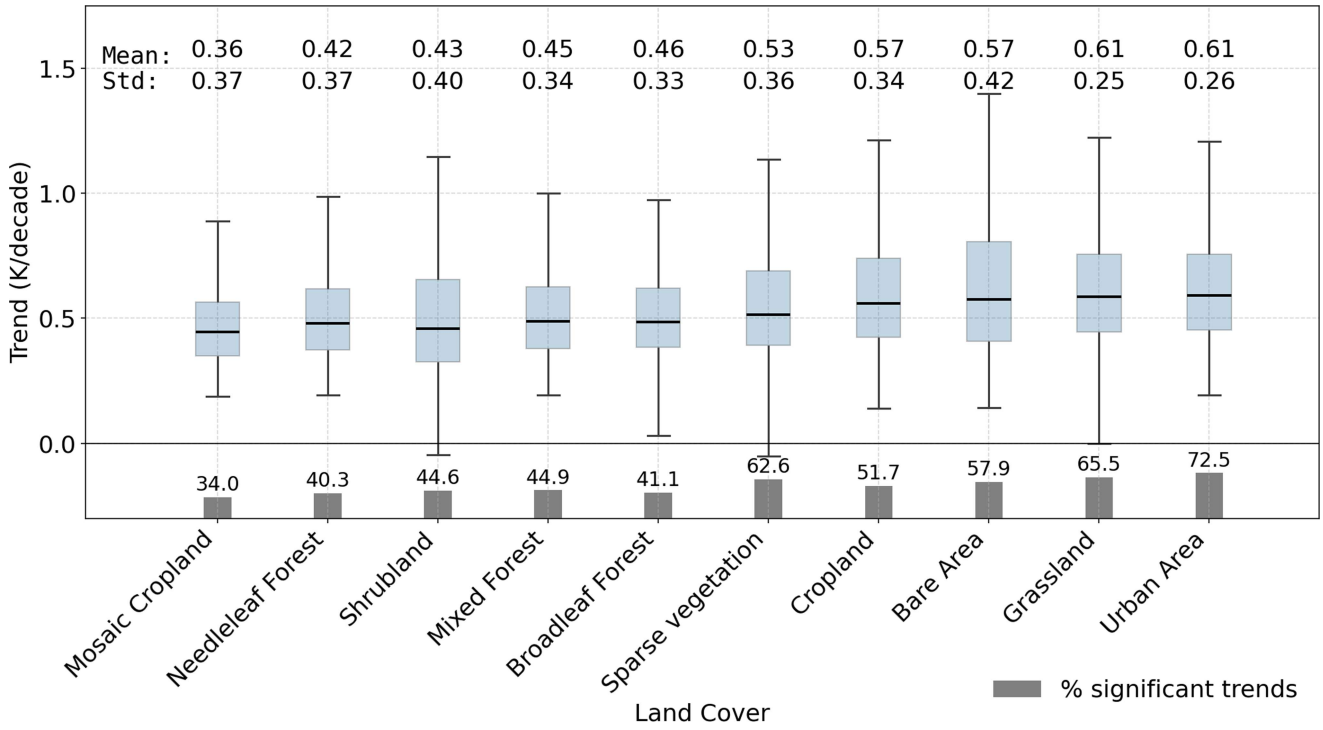

Fig. 10. Significant TIMELINE monthly maximum LST Trends classified by land cover. Bar plot at the bottom: Percentage of each land cover class within the entire study area (green bars) and percentage of significant pixels within each land cover class.

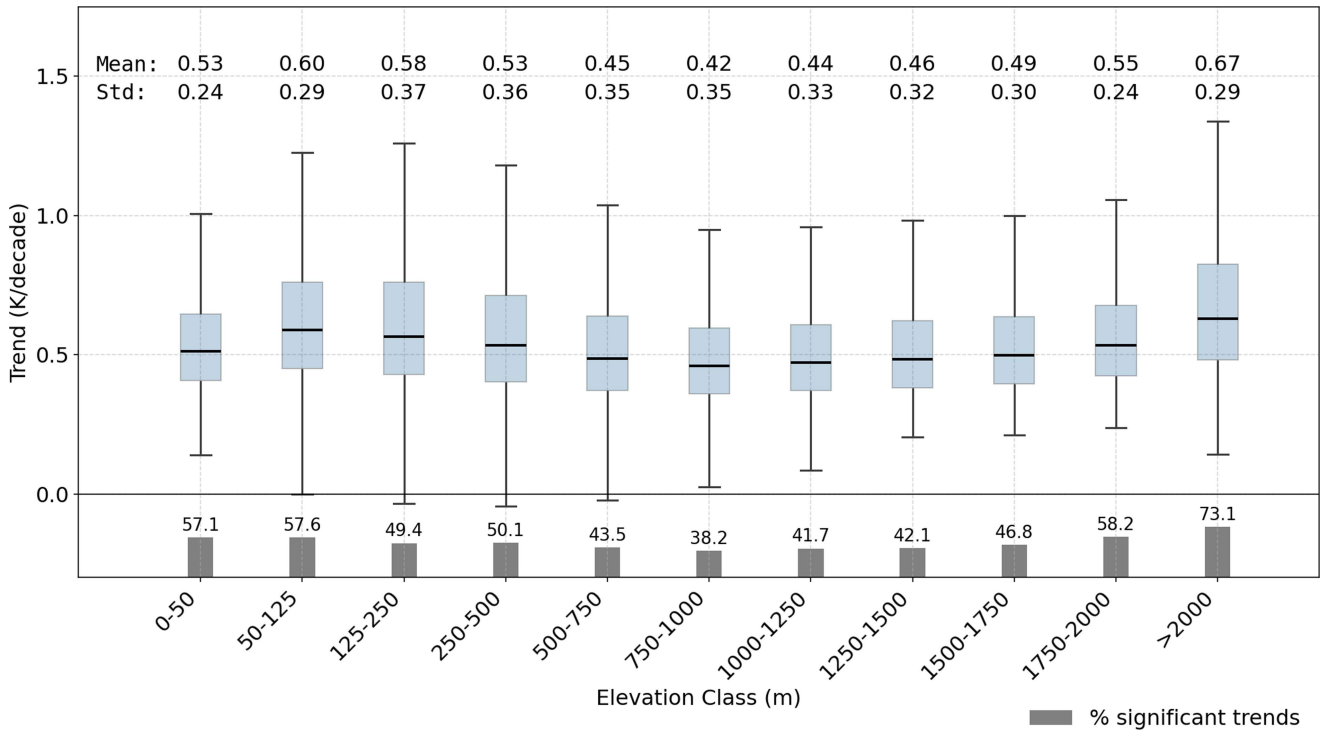

Fig. 11. Significant TIMELINE monthly maximum LST Trends classified by elevation. Bar plot at the bottom: Percentage of each elevation class within the entire study area (green bars) and percentage of significant pixels within each elevation class.

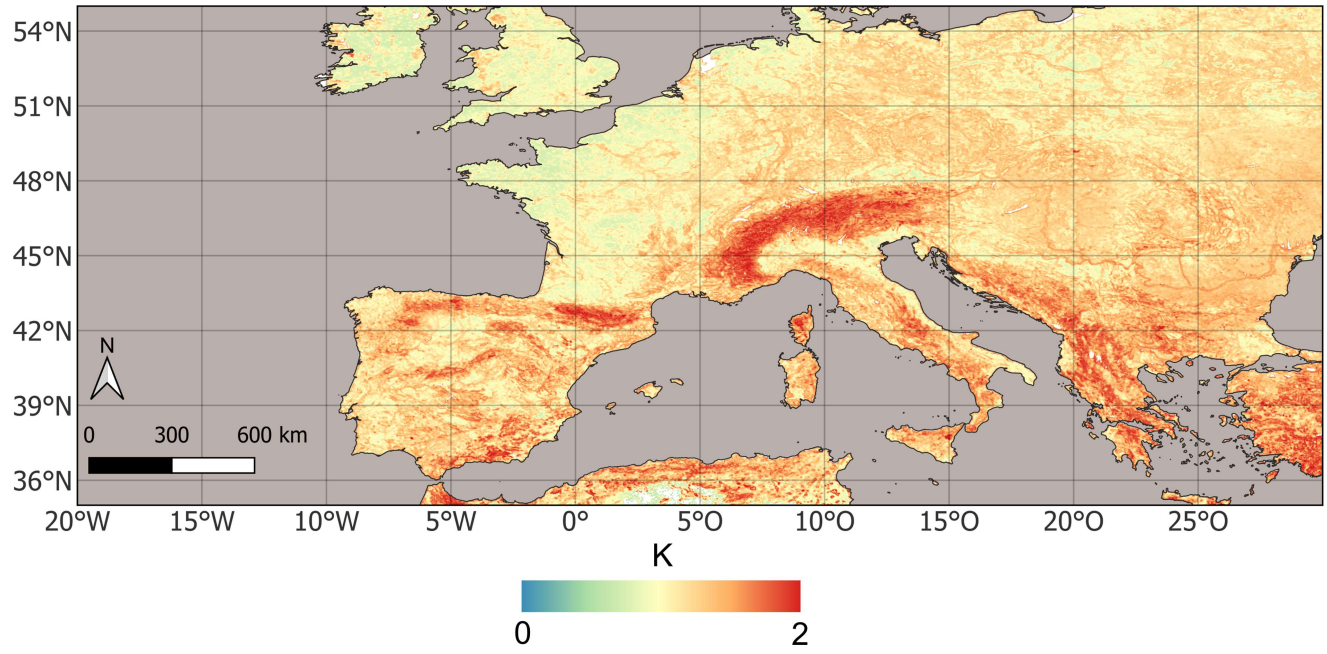

Fig. 12. Mean retrieval uncertainty of TIMELINE LST.

LST data as well as simultaneous observations from different NOAA platforms within the AVHRR LST time series [28]. This resulted in MADs of 2.0 K and 1.9 K, respectively. For the spatial gap-filling, validation was performed in this study by comparing predicted LST values to observed LSTs within a held-out subset of the data. This returned a RMSE of 2.3 K.

It is important to note that validation using independent datasets (such as in situ, MODIS, and CCI LST) is not directly comparable to internal validations within the AVHRR time series, as differences in spatial scale, sensor characteristics, and viewing geometry introduce additional sources of uncertainty. However, the validation results suggest that the subsequent modeling and processing steps required to generate the final analysis-ready monthly maximum LST time series did not significantly increase the overall uncertainty beyond the retrieval uncertainty of the original instantaneous LST.

Although an overall error in the range of 2–2.5 K might appear high when assessing long-term trends of only a few kelvins per decade, it is crucial to consider the amplitude of the underlying monthly maximum LST anomalies, which can be substantially larger. Fig. 13, for example, illustrates the anomalies during the August 2003 heatwave, revealing positive anomaly values of up to 12 K.

B. Comparison With ERA5 and Previous Studies

Another means to assess the validity of the monthly maximum LST results is comparison to analyses with established datasets and findings from previous studies. In this work, we compared the monthly maximum LST anomaly time series to ERA5 SKT anomaly time series. Second, the TIMELINE LST trend results for the whole study area were compared to similarly obtained results from ERA5 SKT.

These comparisons showed that the climatological patterns observed in the AVHRR LST time series aligned well with ERA5 SKT data. However, regarding long-term trend magnitudes, the AVHRR LST series consistently showed higher warming rates than the reference dataset (0.8 K/decade, compared to 0.5 K/decade). In addition, the confidence interval for the TIMELINE AVHRR LST trends was broader (±0.16 K/decade) than that of ERA5 SKT (±0.08 K/decade), suggesting a higher degree of uncertainty in the AVHRR LST trend estimates.

The most plausible explanation for that lies in the nature of the compared variables. As a reanalysis dataset, ERA5 SKT combines satellite observations with air temperature measurements. At both high and low temperature extremes, LST tends to decouple from air temperature, with surface temperatures responding more directly—and often more strongly—to changes in the surface energy balance. This is supported by the larger anomaly amplitudes found in the AVHRR LST series. These higher amplitudes contribute to increased variability and less smoothness in the LST time series, which likely explains not only the higher trend values, but also the lower p-values and broader confidence intervals when compared to ERA5 SKT data. As a result, LST is more sensitive to shifts in climate regimes than near-surface air temperature. A similar argument applies when comparing AVHRR LST with ERA5 SKT: as a reanalysis product, ERA5 SKT combines satellite data with station observations, resulting in a smoother, more conservative trend and smaller anomalies.

Comparing our findings with previous studies on LST trends over Europe, the trend of 0.8 K/decade is higher but within a plausible range. Globally, the reported LST warming rate is 0.3 K/decade for the period 2003–2016 [44] and 0.4 K/decade for the earlier period 1981–1998 [45]. However, Europe is consistently identified as a regional warming hotspot, with local LST trends

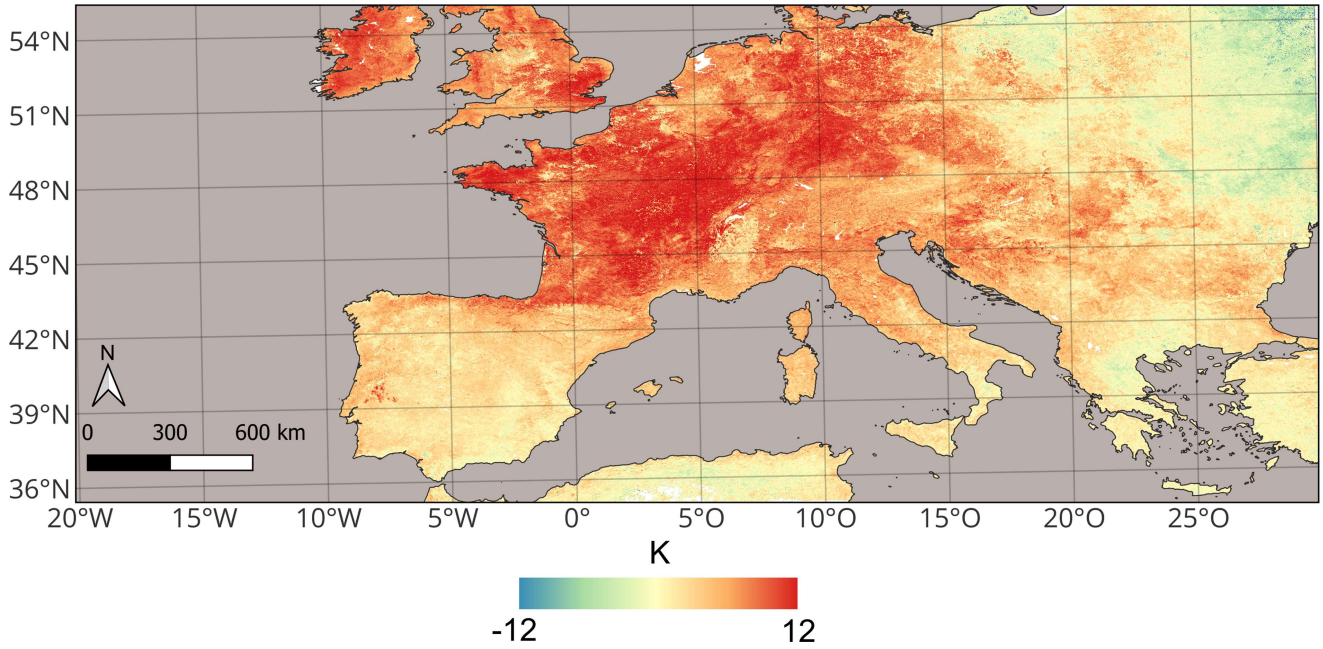

Fig. 13. Monthly maximum LST anomalies during the heatwave in August 2003.

often exceeding 0.5 K/decade. The Copernicus 2024 climate report estimates a European warming rate of approximately 0.5 K/decade based on ERA5 air temperature data [22]. This value aligns with our estimated ERA5 SKT trends used for comparison in this study.

Regarding the spatial patterns, there is broad agreement among these studies that Eastern Europe represents a core hotspot of surface warming. This is fully consistent with our results, which show particularly strong trends across Ukraine, Belarus, and the Hungarian Plains. However, direct comparison of trend magnitudes remains challenging due to differences in time periods and datasets used. Many earlier studies either cover shorter time periods or do not rely exclusively on TIR remote sensing.

C. *Implications of the LST Trend Results*

Urbanization is a well-known driver of LST warming. A large part of the existing research on LST dynamics has focused on the Surface Urban Heat Island effect [46], [47], [48]. Our results also show the highest LST trends for urban areas.

In contrast, the role of croplands in contributing to global warming has received less attention. The results of this study show that croplands—which occupy more than half of the study area—exhibit above-average LST trends and represent a significant component of the overall warming signal across Europe. According to the Copernicus 2024 climate report, a large part of the surface warming in Europe can be attributed to soil moisture deficit, which limits evapotranspiration and results in more energy being converted into sensible heat [22]. This is especially relevant for agricultural areas, as these lack a permanent vegetation layer and are therefore more prone to droughts.

Considering all land cover classes, we find that areas with trees, shrubs or mosaic vegetation have lower positive LST trends compared to areas classified as cropland or grassland. This indicates that heterogeneous landscapes with tree or shrub cover are likely to be less prone to exceptional LST increase. Other studies also reported a negative correlation between NDVI and LST, underscoring the cooling effect of vegetation through evapotranspiration and shading [49].

At the same time, our findings reaffirm the moderating effect of forests on LST trends. Forest areas consistently displayed lower surface warming and fewer statistically significant trends compared to urban and agricultural zones. Despite a possible influence of forest expansion on nighttime warming [26], our results highlight the potential role of forests in mitigating land surface warming in Europe. With their high evapotranspiration rates and surface roughness, they remain an effective buffer against climate change.

Our results further indicate that coastal areas (<50 m a.s.l.) seem to be less impacted by increasing LST compared to regions at higher elevations. These low-lying areas might be affected by coastal influences, such as sea breeze's impact on LST [50] or natural cooling effects [51]. One possible explanation for the comparatively low LST trends in the mid-elevation regions may be the prevalence of forest cover in these regions, which corresponds to observation that forested areas exhibit lower-than-average LST trends. In contrast, the higher trends observed at elevations above 1500 m may be attributed to increasing snow line elevation [52], [53] and glacier retreat [27]. However, it is important to note that mountainous regions are often characterized by complex terrain, which introduces higher uncertainties in the LST retrieval. Consequently, the results at higher elevations—particularly when observed at the AVHRR scale—should be interpreted with caution.

D. Limitations and Outlook

A limitation of all LST products derived from satellite TIR data is the clear sky bias. It describes the missing representation of LST under clouds. Approaches to account for the clear sky bias are still the subject of ongoing research and include the use of shortwave radiation data, in situ measured LST, and passive microwave LST [2]. To overcome this limitation, we based our trend analyses on monthly maximum LST, which is typically observed during clear-sky conditions. As a result, our analyses describe daytime LST trends. Nighttime LST trends might vary [4], [26]. Furthermore, the method used to correct orbital drift for TIMELINE LST Level 3 generation is only valid for areas with stable land cover. This also applies to other ODC methods published in the past [15]. Therefore, the application of LST time series for research on LST dynamics resulting from land cover changes is limited. For the study area of this study, we found that about 91% of the pixels have a stable land cover.

The influence of land cover on LST trends—and more broadly, on climate change—remains an area for future research. While anthropogenic land cover change is widely acknowledged as a driver of global environmental change, its specific impact on surface temperature trends still has to be explored. The long-term, high-resolution AVHRR TIMELINE LST dataset provides a unique opportunity to investigate these land–climate interactions in greater depth. Furthermore, the LST time series at 1 km spatial resolution enables to link land cover types with significant LST anomalies, which will be of high relevance given the heatwaves observed in recent years.

Europe has experienced a number of record summers in recent years, for instance, in 2022 or 2024. To support continued climate and environmental monitoring, it is essential to extend the AVHRR LST time series to cover the most recent years. This extension is currently in progress, involving the processing of data from the MetOp-A and MetOp-B platforms, which succeed the NOAA satellites that carried the AVHRR instrument. Once integrated into the TIMELINE framework, this dataset will provide a powerful basis for addressing open questions regarding climate change in Europe.

V. Conclusion

In this study, we derived monthly maximum LST over central and southern Europe for the period 1986–2018 and analyzed LST trends and their variation for different land cover classes and elevation ranges. These analyses were feasible based on the LST product from the TIMELINE project at DFD of DLR, which provides consistent long-term AVHRR-based environmental products for Europe starting in the early 1980s at an up to daily temporal and 1 km spatial resolution.

The results of the analyses from this study reinforce the reported warming trend across Europe and add detail to the spatial distribution and variation of long-term LST trends. Based on the 1 km resolution data, we found that 40% of the study area showed significant positive LST trends. Strongest trends were observed in eastern Europe (Ukraine, Belarus, Hungarian Plain), on the British Isles, in southern Germany and northern Italy. The TIMELINE LST showed an average trend of $+0.80 \pm 0.16$ K/decade. Comparison to ERA5 SKT revealed a corresponding climatological pattern for both time series, though the ERA5 SKT indicated a more moderate trend of $+0.50 \pm 0.08$ K/decade.

The analysis of LST trends for individual land cover classes showed the highest positive LST trends for urban areas, grasslands and bare areas. Croplands and sparse vegetation also had high average trends of >0.5 K/decade. Forested areas as well as shrublands and mosaic croplands showed comparatively low LST trends. For different elevation ranges, we found that mid-elevation ranges around 1000 m experienced the lowest positive LST trends. Low-lying areas below 50 m also showed comparatively weak trends. The strength of LST trends decreased between 50 and 1000 m and increased again towards higher altitudes above 1000 m.

These results reveal clear differences and patterns of LST trends with respect to different land cover classes and elevation ranges. The low LST increase for low-lying areas might be influenced by an extenuating affect from the ocean in coastal areas, while the low LST trends in mid-elevation ranges are likely to be linked to the prevalence of forest cover in these regions, which showed lower-than-average LST trends. The high positive LST trends observed at high altitudes indicate a high risk of further temperature increase in high mountain areas, leading to accelerated glacier melt and thawing permafrost.

The high LST trends observed for urban areas are in agreement with the established fact that urbanization is a driver of LST warming. However, our results further indicate that croplands substantially contribute to the overall surface warming observed in Europe. On the other hand, areas covered by forests show comparatively low positive LST trends. Thus, our findings reaffirm the moderating effect of forests on LST trends and highlight their potential role in mitigating land surface warming in Europe.

The results of this study contribute to a comprehensive understanding of climate change in Europe. The TIMELINE LST product is currently subject to further development. Data processing for the extension of the time series to more recent years is ongoing, allowing for the analysis of an even longer LST time series in the future.

Acknowledgment

The authors thank the entire TIMELINE team at DFD of DLR for fruitful cooperation and discussion. The authors would also like to thank the DLR headquarters for the funding of the TIMELINE project.

References

[1] G. C. O. System, GCOS WMO Essential Climate Variables. 2023.
[2] P. Reiners, J. Sobrino, and C. Kuenzer, "Satellite-derived land surface temperature dynamics in the context of global change—A review," *Remote Sens.*, vol. 15, 2023, Art. no. 1857.
[3] Z. L. Li et al., "Satellite remote sensing of global land surface temperature: Definition, methods, products, and applications," *Rev. Geophys.*, vol. 61, no. 1, 2023, doi: 10.1029/2022rg000777.
[4] M. R. Ahmed, E. Ghaderpour, A. Gupta, A. Dewan, and Q. K. Hassan, "Opportunities and challenges of spaceborne sensors in delineating land surface temperature trends: A review," *IEEE Sensors J.*, vol. 23, no. 7, pp. 6460–6472, Apr. 2023, doi: 10.1109/Jsen.2023.3246842.

[5] M. X. Zhang et al., "Creating new near-surface air temperature datasets to understand elevation-dependent warming in the Tibetan Plateau," *Remote Sens.*, vol. 12, no. 11, Jun. 2020, Art. no. 1722, doi: 10.3390/rs12111722.

[6] G. Lieberherr and S. Wunderle, "Lake surface water temperature derived from 35 years of AVHRR sensor data for European Lakes," *Remote Sens.*, vol. 10, no. 7, p. 990, Jul. 2018, doi: 10.3390/rs10070990.

[7] S. Dech et al., "Potential and challenges of harmonizing 40 years of AVHRR data: The TIMELINE experience," *Remote Sens.*, vol. 13, no. 18, pp. 1–35, 2021, doi: 10.3390/rs13183618.

[8] C. Eisfelder et al., "Seasonal vegetation trends for Europe over 30 years from a novel normalised difference vegetation index (NDVI) time-series — The TIMELINE NDVI product," *Remote Sens.*, vol. 15, 2023, Art. no. 3616.

[9] S. Rößler and A. J. Dietz, "Detection of snow cover from historical and recent AVHHR data—A thematic TIMELINE processor," *Geomatics*, vol. 2, no. 1, pp. 144–160, Mar. 2022, doi: 10.3390/geomatics2010009.

[10] S. Plank, E.-M. Fuchs, and C. Frey, "A fully automatic instantaneous fire hotspot detection processor based on AVHRR imagery—A TIMELINE thematic processor," *Remote Sens.*, vol. 9, 2017, Art. no. 30.

[11] S. Plank and S. Martinis, "A fully automatic burnt area mapping processor based on AVHRR Imagery-A TIMELINE thematic processor," *Remote Sens.*, vol. 10, 2018, Art. no. 341, doi: 10.3390/rs10020341.

[12] P. Reiners et al., "Validation of AVHRR land surface temperature with MODIS and in situ LST—A TIMELINE Thematic processor," *Remote Sens.*, vol. 13, no. 17, 2021, Art. no. 3473, doi: 10.3390/rs13173473.

[13] P. Reiners, L. Obrecht, A. Dietz, S. Holzwarth, and C. Kuenzer, "First analyses of the TIMELINE AVHRR SST product: Long-term trends of sea surface temperature at 1 km resolution across European Coastal zones," *Remote Sens.*, vol. 16, 2024, Art. no. 1932.

[14] L. Klüser, N. Killius, and G. Gesell, "APOLLO_NG – a probabilistic interpretation of the APOLLO legacy for AVHRR heritage channels," *Atmos. Meas. Techn. Discuss.*, vol. 8, pp. 4413–4449, 2015, doi: 10.5194/amtd-8-4413-2015.

[15] P. Reiners, S. Holzwarth, A. Dietz, M. Bachmann, J. A. Sobrino, and C. Kuenzer, "Fusing AVHRR LST with geostationary SEVIRI LST to create a long-term daily maximum LST time series over Europe," *IEEE J. Sel. Top. Appl. Earth Observ. Remote Sens.*, vol. 18, pp. 2168–2189, 2025, doi: 10.1109/JSTARS.2024.3514734.

[16] C. J. Tomlinson, L. Chapman, J. E. Thornes, and C. Baker, "Remote sensing land surface temperature for meteorology and climatology: A review," *Meteorological Appl.*, vol. 18, no. 3, pp. 296–306, 2011, doi: 10.1002/met.287.

[17] Z. L. Li et al., "Satellite remote sensing of global land surface temperature: Definition, methods, products, and applications," *Rev. Geophys.*, vol. 61, no. 1, pp. 1–77, Mar. 2023, doi: 10.1029/2022RG000777.

[18] X. L. Zhu et al., "Reconstruction of land surface temperature under cloudy conditions from Landsat 8 data using annual temperature cycle model," *Remote Sens. Environ.*, vol. 281, 2022, Art. no. 113261, doi: 10.1016/j.rse.2022.113261.

[19] L. Q. Hu, Y. Sun, G. Collins, and P. Fu, "Improved estimates of monthly land surface temperature from MODIS using a diurnal temperature cycle (DTC) model," *ISPRS J. Photogrammetry Remote Sens.*, vol. 168, pp. 131–140, Oct. 2020, doi: 10.1016/j.isprsjprs.2020.08.007.

[20] L. Alexander et al., "Global observed changes in daily climate extremes of temperature and precipitation," *J. Geophysical Res.*, vol. 111, pp. 1–22, 2006, doi: 10.1029/2005JD006290.

[21] P. M. Forster et al., "Indicators of global climate change 2024: Annual update of key indicators of the state of the climate system and human influence," *Earth Syst. Sci. Data*, vol. 17, no. 6, pp. 2641–2680, 2025, doi: 10.5194/essd-17-2641-2025.

[22] C. C. C. S. (C3S) and W. M. O. (WMO), "European state of the climate 2024," Copernicus Climate Change Service (C3S) and World Meteorological Organization (WMO), 2025. [Online]. Available: climate.copernicus.eu/ESOTC/2024

[23] L. Jaime, E. Batllori, and F. Lloret, "Bark beetle outbreaks in coniferous forests: A review of climate change effects," *Eur. J. Forest Res.*, vol. 143, no. 1, pp. 1–17, 2024, doi: 10.1007/s10342-023-01623-3.

[24] M. Chiriaco, S. Bastin, P. Yiou, M. Haeffelin, J.-C. Dupont, and M. Stéfanon, "European heatwave in July 2006: Observations and modeling showing how local processes amplify conducive large-scale conditions," *Geophysical Res. Lett.*, vol. 41, no. 15, pp. 5644–5652, 2014, doi: 10.1002/2014GL060205.

[25] N. Christidis, G. S. Jones, and P. A. Stott, "Dramatically increasing chance of extremely hot summers since the 2003 European heatwave," *Nature Climate Change*, vol. 5, no. 1, pp. 46–50, 2015, doi: 10.1038/nclimate2468.

[26] E. Ghaderpour, P. Mazzanti, F. Bozzano, and G. S. Mugnozza, "Trend analysis of MODIS land surface temperature and land cover in Central Italy," *Land*, vol. 13, no. 6, p. 796, 2024.

[27] D. T. Gök, D. Scherler, and H. Wulf, "Land surface temperature trends derived from Landsat imagery in the Swiss Alps," *Cryosphere*, vol. 18, no. 11, pp. 5259–5276, Nov. 2024, doi: 10.5194/tc-18-5259-2024.

[28] P. Reiners, S. Holzwarth, J. Sobrino, and C. Kuenzer, "Long-term trends of land surface temperature over Europe derived from a daytime normalized AVHRR time series," in *Proc. 7th Int. Symp. Recent Adv. Quantitative Remote Sens.*, pp. 1–17, 2024.

[29] S. Asam, C. Eisfelder, A. Hirner, P. Reiners, S. Holzwarth, and M. Bachmann, "AVHRR NDVI compositing method comparison and generation of multi-decadal time series—A TIMELINE thematic processor," *Remote Sens.*, vol. 15, no. 6, 2023, Art. no. 1631, doi: 10.3390/rs15061631.

[30] J. Danielson and D. Gesch, "Global multi-resolution terrain elevation data 2010 (GMTED2010)," 2011.

[31] C. Eisfelder et al., "Thirty-year analyses of seasonal NDVI and climatic drivers across different land cover types and biogeographical regions in Europe," *IEEE J. Sel. Top. Appl. Earth Observ. Remote Sens.*, vol. 18, pp. 11225–11249, 2025, doi: 10.1109/JSTARS.2025.3558816.

[32] P. Sismanidis, B. Bechtel, I. Keramitsoglou, F. Göttsche, and C. T. Kiranoudis, "Satellite-derived quantification of the diurnal and annual dynamics of land surface temperature," *Remote Sens. Environ.*, vol. 265, 2021, Art. no. 112642, doi: 10.1016/j.rse.2021.112642.

[33] C. Yoo, J. Im, D. Cho, N. Yokoya, J. Xia, and B. Bechtel, "Estimation of all-weather 1 km MODIS land surface temperature for humid summer days," *Remote Sens.*, vol. 12, no. 9, 2020, Art. no. 1398.

[34] W. Zhao and S.-B. Duan, "Reconstruction of daytime land surface temperatures under cloud-covered conditions using integrated MODIS/Terra land products and MSG geostationary satellite data," *Remote Sens. Environ.*, vol. 247, 2020, Art. no. 111931, doi: 10.1016/j.rse.2020.111931.

[35] H. B. Mann, "Nonparametric tests against trend," *Econometrica*, vol. 13, no. 3, pp. 245–259, 1945, doi: 10.2307/1907187.

[36] M. Kendall, *Rank Correlation Measures*, vol. 202, no. 15, London, U.K.: Charles Griffin, 1975.

[37] H. Theil, *A Rank-Invariant Method of Linear and Polynomial Regression Analysis*. Berlin, Germany: Springer, 1992, pp. 345–381.

[38] P. K. Sen, "Estimates of the regression coefficient based on Kendall's Tau," *J. Amer. Stat. Assoc.*, vol. 63, no. 324, pp. 1379–1389, 1968, doi: 10.1080/01621459.1968.10480934.

[39] J. R. Eastman et al., "Seasonal trend analysis of image time series," *Int. J. Remote Sens.*, vol. 30, no. 10, pp. 2721–2726, 2009, doi: 10.1080/01431160902755338.

[40] S. M. Vicente-Serrano et al., "Vegetation greening in Spain detected from long term data (1981?2015)," *Int. J. Remote Sens.*, vol. 41, no. 5, pp. 1709–1740, Mar. 2020, doi: 10.1080/01431161.2019.1674460.

[41] J. Zeder and E. M. Fischer, "Observed extreme precipitation trends and scaling in Central Europe," *Weather Climate Extremes*, vol. 29, 2020, Art. no. 100266, doi: 10.1016/j.wace.2020.100266.

[42] G. Zittis, A. Bruggeman, and J. Lelieveld, "Revisiting future extreme precipitation trends in the Mediterranean," *Weather Climate Extremes*, vol. 34, 2021, Art. no. 100380, doi: 10.1016/j.wace.2021.100380.

[43] Z. Q. Wang et al., "Large discrepancies of global greening: Indication of multi-source remote sensing data," *Glob. Ecol. Conservation*, vol. 34, 2022, Art. no. e02016, doi: 10.1016/j.gecco.2022.e02016.

[44] J. Sobrino, S. García-Monteiro, and Y. Julien, "Surface temperature of the planet earth from satellite data over the period 2003–2019," *Remote Sens.*, vol. 12, no. 12, 2020, Art. no. 2036, doi: 10.3390/rs12122036.

[45] M. Jin and R. E. Treadon, "Correcting the orbit drift effect on AVHRR land surface skin temperature measurements," *Int. J. Remote Sens.*, vol. 24, no. 22, pp. 4543–4558, 2010, doi: 10.1080/0143116031000095943.

[46] A. Rasul et al., "A review on remote sensing of urban heat and cool islands," *Land*, vol. 6, no. 2, 2017, Art. no. 38, doi: 10.3390/land6020038.

[47] K. Deilami, M. Kamruzzaman, and Y. Liu, "Urban heat island effect: A systematic review of spatio-temporal factors, data, methods, and mitigation measures," *Int. J. Appl. Earth Observ. Geoinformation*, vol. 67, pp. 30–42, 2018, doi: 10.1016/j.jag.2017.12.009.

[48] D. Zhou et al., "Satellite remote sensing of surface urban heat islands: Progress, challenges, and perspectives," *Remote Sens.*, vol. 11, no. 1, 2018, Art. no. 48, doi: 10.3390/rs11010048.

[49] Y. Kara and V. Yavuz, "Urban microclimates in a warming world: Land surface temperature (LST) trends across ten major cities on seven continents," *Urban Sci.*, vol. 9, no. 4, 2025, Art. no. 115.

[50] L. S. Chen, Y. Zhang, E. Y. Zhu, Y. Che, and Y. Y. Wu, "Segregation of sea breezes and cooling effects on land-surface temperatures in a coastal city," *Sustain. Cities Soc.*, vol. 118, 2025, Art. no. 106017, doi: 10.1016/j.scs.2024.106017.
[51] I. Ontel, V. Amihaesei, D. Micu, A. Dumitrescu, and S. Cheval, "Influence of environmental factors on land surface temperature and surface urban heat island. A cross-country analysis in Romania," *Sustain. Cities Soc.*, vol. 128, 2025, Art. no. 106454, doi: 10.1016/j.scs.2025.106454.
[52] Z. Y. Hu et al., "Snow moving to higher elevations: Analyzing three decades of snowline dynamics in the Alps," *Geophysical Res. Lett.*, vol. 47, no. 12, Jun. 2020, Art. no. e2019GL085742, doi: 10.1029/2019GL085742.
[53] J. Koehler, A. Bauer, A. J. Dietz, and C. Kuenzer, "Towards forecasting future snow cover dynamics in the European Alps-the potential of long optical remote-sensing time series," *Remote Sens.*, vol. 14, no. 18, Sep. 2022, Art. no. 4461, doi: 10.3390/rs14184461.
[54] ESA, "Land cover CCI product user guide version 2. Tech. Rep," Accessed: Sep. 19, 2024. [Online]. Available: maps.elie.ucl.ac.be/CCI/viewer/download/ESACCI-LC-Ph2-PUGv2_2.0.pdf

Christina Eisfelder received the Dipl.-Ing. and Ph.D. (Dr.-Ing.) degrees in cartography from the Technical University of Dresden, Dresden, Germany, in 2008 and 2013, respectively.

Her diploma thesis dealt with object-based forest type mapping based on very-high-resolution optical remote sensing data. Her dissertation was on modeling net primary productivity and above-ground biomass for mapping of spatial biomass distribution in Kazakhstan. Since 2008, she has been with the German Remote Sensing Data Center (DFD), German Aerospace Center (DLR), Oberpfaffenhofen, Germany. As a Research Scientist within the Department "Land Surface Dynamics," she has been involved in several international research projects. Her current research interests include remote sensing analyses in the context of vegetation dynamics and land surface monitoring, land cover and crop type mapping, phenological analyses, long time-series and trend analyses, and drought monitoring and early warning.

Philipp Reiners received the M.Sc. degree in physical geography from the University of Marburg, Marburg, Germany, in 2019 and the Dr. rer. nat. in geography from Julius-Maximilians-University Würzburg, Würzburg, Germany, in 2025.

From 2019 to 2024, he worked as a Research Scientist with the Land Surface Department, the German Aerospace Center (DLR), German Remote Sensing Data Center (DFD), Wessling, Germany. During this time, he developed a 40-year-long-term data record of land and sea surface temperature from AVHRR data over Europe and North Africa. Since April 2025, he has been a Research Associate with the GFZ Helmholtz Centre for Geosciences in Potsdam, Germany, in the Remote Sensing and Geoinformatics Section, where he works on hyperspectral remote sensing and the EnMAP mission. His research interests include thermal remote sensing, climatology, time-series analysis, and calibration and validation.

Claudia Kuenzer received the Diploma (M.Sc.) degree in geography from the University of Trier, Trier, Germany, in 2001, and the Ph.D. degree in remote sensing from the TU Vienna, Vienna, Austria, in 2005.

She is currently a Professor of Remote Sensing and Geosciences. Since 2016, she has been the Head of the Department "Land Surface Dynamics" with the Earth Observation Center, German Aerospace Center, Oberpfaffenhofen, near Munich, Germany. From 2001 to 2006, she was a Research Associate with the German Remote Sensing Data Center, German Aerospace Center, Germany. In 2005, she spent half a year as a Guest Scientist with the Institute of Remote Sensing Applications, and Beijing Normal University, Beijing, China. From 2006 to 2008, she held a position as a Postdoc Scientist and an Institute Assistant with the Institute of Photogrammetry and Remote Sensing, TU Vienna. Since 2008, she has been back with the Earth Observation Center, where she acted as a Research Group Leader and a Science Coordinator of several large interdisciplinary international projects. She currently supervises 12 Ph.D. students and two habilitation candidates. She has contributed to more than 200 SCI journal papers and more than 250 conference proceedings. Her research interests include remote sensing applications for the assessment of land surface dynamics based on long-time series analyses and innovative AI methods.